

Two-dimensional resonant piston-like sloshing in a moonpool

Odd M. Faltinsen **Olav F. Rognebakke** **Alexander N. Timokha**
 Odd.Faltinsen@ntnu.no Olav.Rognebakke@dnv.com Alexander.Timokha@ntnu.no

Centre for Ships and Ocean Structures
Norwegian University of Science and Technology
NO-7491 Trondheim, Norway

The fluid inside of moonpools, between the hulls of multi-hull vessels and between ships in a side-by-side arrangement in waves may show considerable piston-like resonant motions. The possibility of trapped modes has relevance. Examples on references on trapped modes are McIver et al. (2003); McIver (2005); Kuznetsov et al. (2002). Our present theoretical and experimental studies are limited to two-dimensional flow. Small-amplitude vertical motions of

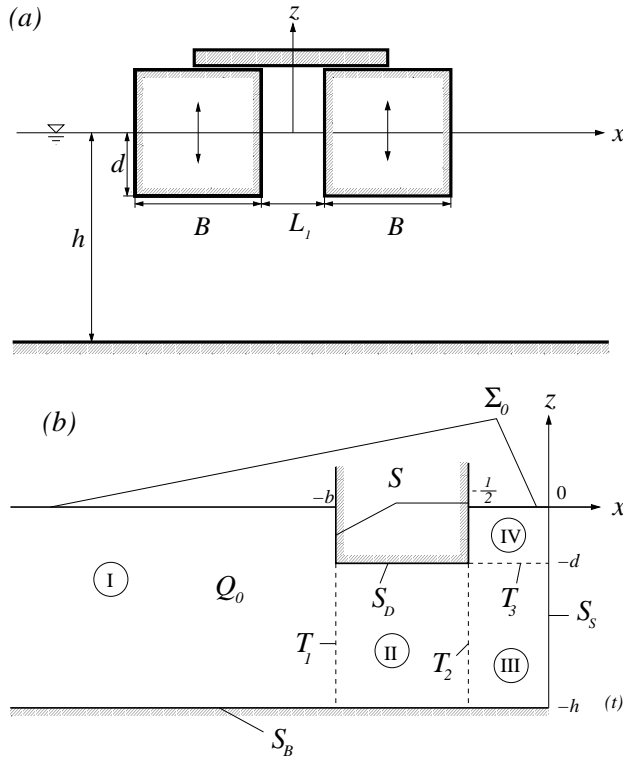


Figure 1: General geometrical sketch (a) and definitions of the dimensionless problem (b).

the two rigidly connected rectangular hulls in Fig. 1 (a) are studied by linear potential flow theory. The geometrical dimensions are scaled by the horizontal width of the moonpool L_1 . The non-dimensional time is σt where σ is the circular forcing frequency. Further, we define $\Lambda := \frac{\sigma^2 L_1}{g}$ where g is the gravity acceleration. The heave amplitude divided by L_1 is denoted ε .

Because of the Oz -symmetry only fluid motions in the left to the Oz -axis are considered as shown in Fig. 1 (b). The fluid domain Q_0 is divided into four subdomains *I*, *II*, *III* and *IV* by auxiliary interfaces T_1 , T_2 and T_3 as shown in

Fig. 1 (b). The velocity potential is expressed as

$$\varphi^{(1)}(x, z) \cos t + \varphi^{(2)}(x, z) \sin t. \quad (1)$$

Further, pursuing independent boundary value problems in these subdomains, we define the Neumann traces of $\varphi^{(i)}$ on T_j , $j = 1, 2, 3$, $i = 1, 2$ as follows

$$T_1: \quad \frac{\partial \varphi^{(i)}}{\partial x}(-b, z) = w_1^{(i)}(z) \quad -h < z < -d, \quad (2a)$$

$$T_2: \quad \frac{\partial \varphi^{(i)}}{\partial x}(-\frac{1}{2}, z) = w_2^{(i)}(z) \quad -h < z < -d, \quad (2b)$$

$$T_3: \quad \frac{\partial \varphi^{(i)}}{\partial z}(x, -d) = w_3^{(i)}(x) \quad -\frac{1}{2} < x < 0. \quad (2c)$$

Green functions are derived for each subdomain. The velocity potentials for *I*, *II*, *III* and *IV* are separately expressed in terms of distributions of $w_j^{(i)}$ and the appropriate Green function along T_j . Integral equations with respect to $w_j^{(i)}$ follow by using the Dirichlet transmission conditions on T_j . In addition, the continuity of fluid mass is satisfied separately for domains *II* and *III*. An inhomogeneous system of ten integral equations is the result. This is solved by a Galerkin method by expressing

$$w_1^{(i)}(z) = \sum_{j=1}^{N_1} \alpha_j^{(1,i)}(z) v_j^{(1)}(z); \quad w_2^{(i)}(z) = \sum_{j=1}^{N_2} \alpha_j^{(2,i)}(z) v_j^{(1)}(z)$$

$$w_3^{(i)}(x) = \sum_{j=1}^{N_3} \alpha_j^{(3,i)}(x) v_j^{(2)}(x), \quad i = 1, 2, \quad (3)$$

where $\{v_i^{(1)}\}$ and $\{v_i^{(2)}\}$ are two complete systems of functions on $(-h, -d)$ and $(-\frac{1}{2}, 0)$, respectively. The result is a system of M linear algebraic systems with respect to M variables, i.e

$$\mathcal{P}B = \varepsilon b. \quad (4)$$

The matrix \mathcal{P} has the following structure

$$\mathcal{P} = \left\| \begin{array}{c|c} D & -p \\ \hline p & D \end{array} \right\|, \quad (5)$$

where the two sub-matrices D and p have dimensions $(\frac{M}{2}) \times (\frac{M}{2})$ and $N_1 \times N_1$, respectively. N_1 is the number of terms

used in the approximation of w_1 . The limited space does not permit a detailed explanation of the sub-matrices.

Convergence and accuracy of the Galerkin method depend on the functional sets $\{v_j^{(1)}(z)\}$ and $\{v_j^{(2)}(x)\}$. Because the Neumann traces on T_k , $k = 1, 2, 3$ are singular at the corner points of the rectangular body, the use of a smooth functional basis, i.e. trigonometrical or polynomial, may cause weak convergence. On the contrary, accounting for the singular character of the traces improves the convergence (Porter & Evans, 1995; Kuznetsov et al., 2001). The following functional sets

$$\begin{aligned} v_j^{(1)}(z) &= \frac{1}{r_j^{(1)}} \left(1 - \left(\frac{z+h}{h-d} \right)^2 \right)^{m_j}; \\ v_j^{(2)}(x) &= \frac{1}{r_j^{(2)}} (1 - (2x)^2)^{m_j}, \quad j \geq 1, \end{aligned} \quad (6)$$

with $m_j \in \{\pm\frac{1}{3} + j - 1, j \geq 1\}$ are therefore used. Here $r_j^{(1)}$ and $r_j^{(2)}$ are normalization factors.

The functional basis (6) makes it possible to get analytical expressions for elements of \mathcal{P} and b in terms of the gamma- and Bessel functions. The solution guarantees a fast convergence and provides about 5-7 significant figures with only 5-6 basis functions on each transmission interface. The accurate prediction of the singularities at the corners is also essential in matching with the local vortex shedding model by Graham (1980).

Non-unique solutions of the boundary value problem for a certain value of Λ is associated with existence of trapped mode solutions, which appear as non-trivial solutions of the corresponding homogeneous problem.

A necessary existence condition for the piston-like trapped mode solution is

$$\det \|D(\Lambda_*)\| = 0 \quad \text{for a certain} \quad \Lambda_* \in \left(0, \frac{\pi}{2} \tanh \left(\frac{\pi}{2} \right) \right). \quad (7)$$

This condition yields a non-trivial solution of the homogeneous problem

$$D(\Lambda_*)\mathbf{B}_1 = \mathbf{0}. \quad (8)$$

If $w_1^{(1)}(z)$, $i = 1, 2$, determined by this non-trivial solution satisfy the conditions of zero far-field wave amplitude $\mathcal{A}_0^{(1)}$ and non-zero flux over the moonpool, the problem has the piston-like trapped mode at the ‘‘resonant frequency’’ Λ_* .

After identifying the resonant frequencies Λ_* and finding non-trivial solutions from (8), we can numerically detect geometrical configurations with B , h and d for which (8) implies the existence of a trapped mode. By defining the ratio

$$\mathcal{J}(d, B, h) = \mathcal{A}_0^{(1)} / \mathcal{A}_1^{(1)}, \quad (9)$$

where $\mathcal{A}_1^{(1)} \neq 0$ is the space-averaged wave amplitude in the moonpool, we conducted tedious numerical studies to find the trapped modes, i.e. (d, B, h) for which $\mathcal{J} = 0$. These showed that the \mathcal{J} 's are finite and positive, much larger than the maximum numerical error estimated as $\leq 10^{-6}$, at least, for geometric shapes related to our experimental

cases. Typical behaviour of \mathcal{J} versus the draught d for different values of B is illustrated in Figs 2 (a,b). \mathcal{J} tends to zero only as $d \rightarrow h$, but this case is not of our present interest. In contrast, when $d \rightarrow 0$ and $B \rightarrow 0$ (thin structure or wide moonpool in deep water), the transcendental equation (7) may have no roots, i.e. no resonant frequencies. The last fact is demonstrated in Figures 2 (a,b) for $B = 0.2$ by the existence of a finite interval between the graphs and the vertical axis.

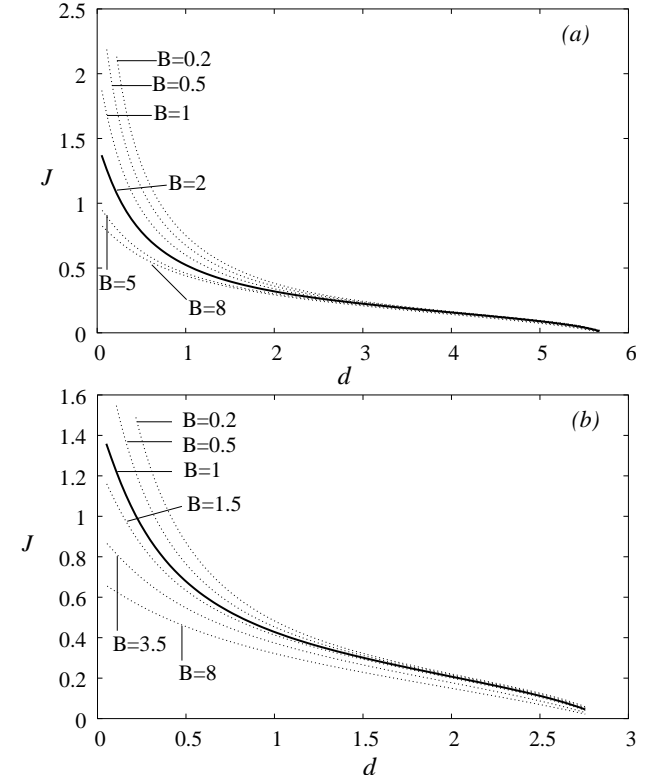


Figure 2: The ratio \mathcal{J} defined by (9) versus the draught d for $h = 5.72222$ (a) and $h = 2.86111$ (b) and different breadths B of the rectangular side hulls. Solid lines correspond to model tests. All lengths are normalized by L_1 .

Model tests

Moonpool model tests have been performed in a wave flume that is 0.6m wide and has a water depth of 1.03m and a total length of 13.5m. The flow-field is approximately two-dimensional. The width of the two rectangular parts of the ship hull, B , is 0.36m.

Figure 3 shows the position of the wave probes, position gauges and accelerometers in one of the test configurations. A total of twelve wave probes were used, denoted w1-w12. For most of the forcing frequencies, some initial beating occurs in the moonpool. The free surface elevation inside the moonpool reaches the absolute maximum and minimum in the middle, but the difference in level across the moonpool is small. The minimum amplitude for radiated waves is observed for frequencies slightly higher than the frequency causing the maximum free surface elevation inside the moonpool. The measured steady state free surface elevation is in general quite sinusoidal. Vortex shedding at

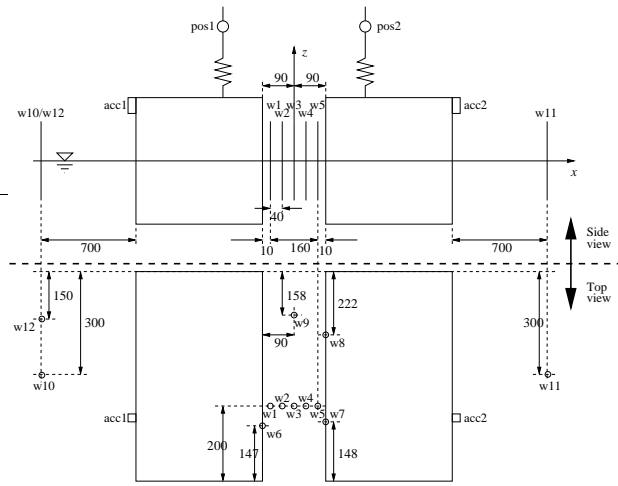


Figure 3: Instrumentation when the moonpool width and depth are $L_1 = 180\text{mm}$ and $d = 180\text{mm}$, respectively. All measures in (mm).

the right corners of the rectangular ship hulls was clearly observed for a large free surface motion in the moonpool.

The following sets of model tests were performed

Case 1: $h = 5.72222$, $d = 1$ and $B = 2$ with the two non-dimensional heave amplitudes $\varepsilon = 0.013889$ and 0.027778 ;

Case 2: $h = 5.72222$, $d = 1.5$ and $B = 2$ with the same two heave amplitudes and

Case 3: $h = 2.86111$, $d = 0.5$ and $B = 1$ with only one non-dimensional heave amplitude $\varepsilon = 0.00694$.

Comparison with experiments

The theoretical and experimental piston mode resonance frequency compares well. The experiments are equal to our theory in Case 1 (Fig. 4a), while there are small differences in Case 2 and 3, which are hardly visible in Fig. 4. The value Λ_* was weakly dependent on the forcing amplitude. The agreement with the theory by Molin (2001) is illustrated in Fig. 4. The discrepancy increases when the draught is small relative to the moonpool width.

Measurements of the piston-like space-averaged wave elevations in the moonpool and far away from the structure (henceforth, we focus only on measuring probe w11) make it possible to validate the linear theoretical predictions. Both the experimental and theoretical values are scaled by the forcing amplitude. The experimental and theoretical phase-lags θ_m and θ_p relative to the heave motion are also evaluated. Results are presented in Fig. 5. The agreement between the experiments and the linear theory is reasonable for the smallest heave amplitudes (Fig. 5). A discrepancy for the maximum response (resonance at $\Lambda = \Lambda_*$) is partly due to vortex shedding at the corners of the rectangular hulls. An interesting point is the behaviour of the experimental values at j_1 , where, we believe, other nonlinearities than due to the vortex shedding yield a jump in the response curves. This jump changes the structure of the branching, which becomes (as shown by arrows) parallel to the linear prediction. As shown in Fig. 5, increasing forcing amplitude decreases the scaled experimental amplitudes, so that jump-like behaviour at j_1 changes to a ‘‘shelf’’

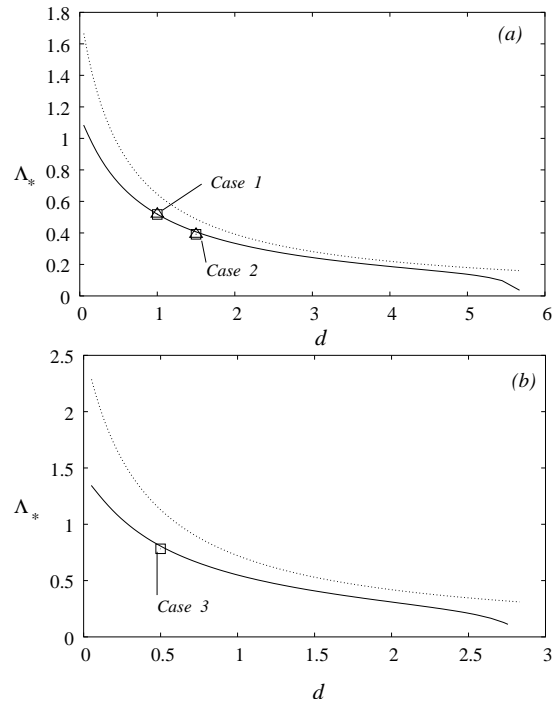


Figure 4: Theoretical prediction of the resonance frequency Λ_* (root of (7)) versus d (solid line) and the estimate by Molin (2001) (dotted line). The part (a) is related to Cases 1-2 ($h = 5.72222$ and $B = 2$), but (b) implies Case 3 ($h = 2.86111$ and $B = 1$). The square and triangle centres mark the experimental values of Λ_* for lower forcing amplitudes ($\varepsilon = 0.013889$ in (a) and $\varepsilon = 0.006944$ in (b)) and larger forcing amplitudes ($\varepsilon = 0.02778$), respectively.

on the response curves.

Cases 1 and 2 indicate that, to some extent, the agreement may be improved if damping due to vortex shedding is accounted for. Case 3 in Fig. 6 presents elevation measurements that cannot be fully explained by vortex shedding. The experiments show a higher resonant response than found by our theory. A drift s of the maximum response is seen. A similar but smaller drift was also observed for Case 2. In contrast to the ‘‘smooth’’ branches of the linear theory, the experiments in Case 3 identify a jump j_4 to the left of the primary resonance Λ_* . A novelty is also a jump to the right of the Λ_* , occurring at j_3 . Figure 7 shows the time record of the measured elevation at w1 and w5 for Case 3 at the point j_3 in Fig. 6. The unfiltered signal is periodic, but clearly non-sinusoidal due to the presence of higher harmonics. A band-pass filtering shows the pronounced harmonic component with a frequency four times the forcing frequency. A logical explanation of this higher harmonic may be internal (secondary) resonance between the piston-like mode $\Lambda_* = 0.8041$ and a sloshing mode having the non-dimensional resonant frequencies Λ_i , $i \geq 1$. Because the piston-like mode may create only a parametric-type resonance for the sloshing modes and the resonant sloshing frequencies always are quite larger than the lowest, piston-like Λ_* , the secondary resonance in terms of a non-linear theory, which produces $l\sigma$, $l = 1, 2, \dots$ -harmonics, is predictable when $l\sigma/\sigma_i$, $l \geq 1$, $i \geq 1$ is an integer number. Thinking in terms of the lowest l and i and using estimates

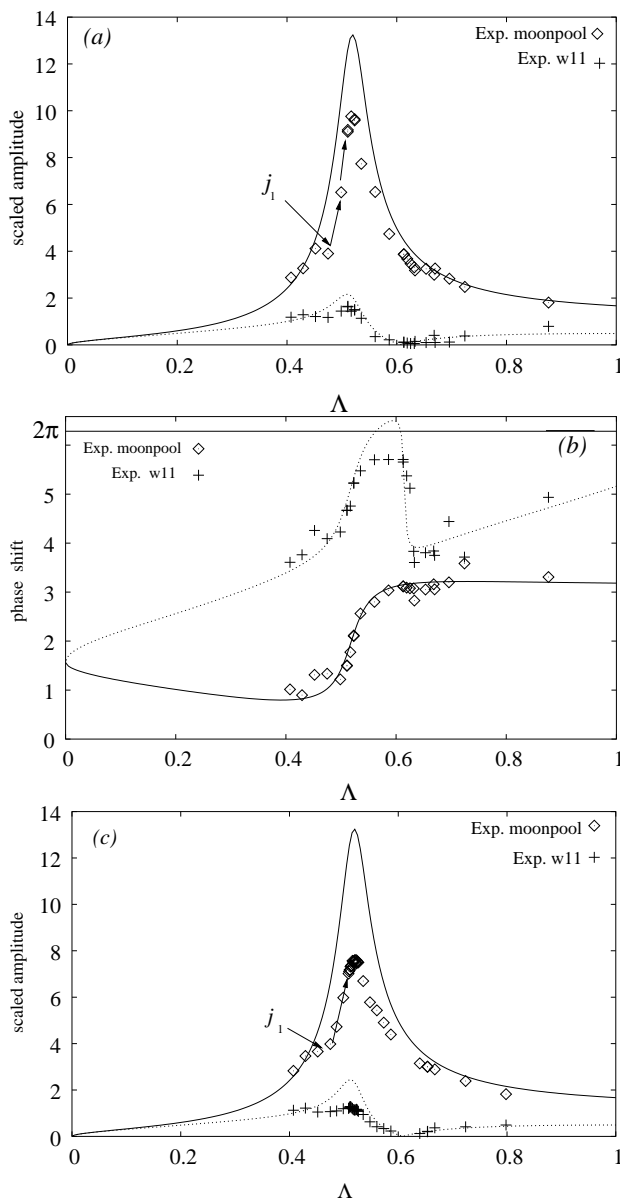


Figure 5: Case 1 with $B = 2$, $d = 1$ and $h = 5.72222$. Theoretical and experimental amplitudes of the piston-like motions and the wave elevation at w11 (scaled by the forcing amplitude) versus Λ are presented in (a,c). Theoretical values for the moonpool are space-averaged. The theoretical and experimental phase-shifts θ_m and θ_p are given in (b). Parts (a,b) compare theory and experiments for the experimental forcing amplitude $\varepsilon = 0.013889$, but (c) imply $\varepsilon = 0.027778$.

of the resonant sloshing frequencies by Molin (2001), we find that $l\sigma/\sigma_i \approx \sqrt{l/2i}$ for Λ_* in Case 3. Possible “resonance” combinations are $l = 2, i = 1, l = 4, i = 1, l = 4, i = 2$ etc. Special studies are needed to select from these combinations an actual secondary resonance.

Our next step in the theoretical analysis is to incorporate the local vortex shedding model by Graham (1980).

References

GRAHAM, J.M.R. 1980 The forces on sharp-edged cylinders in oscillatory flow at low Keulegan-Carpenter num-

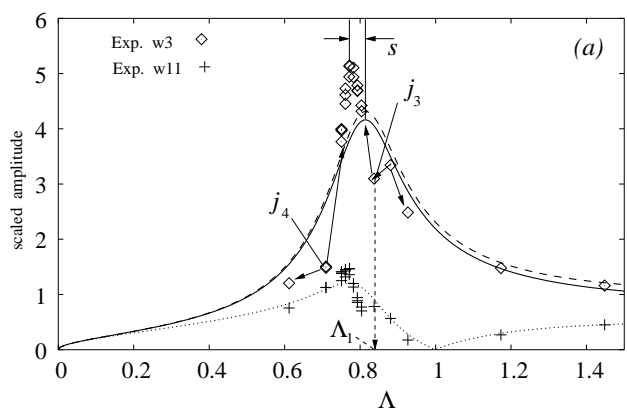


Figure 6: The same as in Fig. 5 (a,c), but for $B = 1$, $d = 0.5$, $h = 2.86111$ and the experimental forcing amplitude $\varepsilon = 0.006944$. The dashed line corresponds to the scaled theoretical wave elevations at w3.

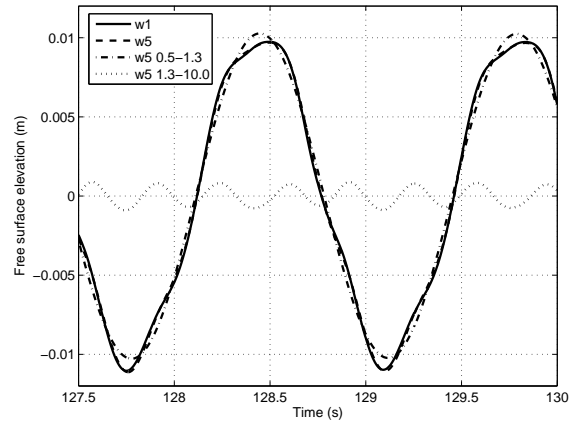


Figure 7: Dimensional steady-state elevations at w1 (solid line), w5 (dashed line) as well as their Fourier filtering in the range 0.5-1.3Hz (dot-and-dashed line) and 1.3-10Hz (dotted line). The figure corresponds to j_3 in Fig. 6 (a) with $\Lambda = 0.8041$ (0.745Hz).

bers. *J. Fluid Mech.* **97**, part 1, 331–346.

KUZNETSOV, N., MCIVER, P., LINTON, C.M. 2001 On uniqueness and trapped modes in the water-wave problem for vertical barriers. *Wave Motion* **33**, 283-307.

KUZNETSOV, N., MAZ'YA, V., VAINBERG, B. 2002 *Linear water waves. A Mathematical approach* Cambridge University Press.

MCIVER, P. 2005 Complex resonances in the water-wave problem for a floating structure. *J. Fluid Mech.* **536**, 423–443.

MCIVER, P., MCIVER, M., ZHANG, J. 2003 Excitation of trapped water waves by the forced motion of structures. *J. Fluid Mech.* **494**, 141-162.

MOLIN, B. 2001 On the piston and sloshing modes in moonpools. *J. Fluid Mech.*, **430**, 27-50.

PORTER, R., EVANS, D.V. 1995 Complementary approximations to wave scattering by vertical barriers. *J. Fluid Mech.* **294**, 155–180.

Faltinsen, O.M., Rogenbakke, O.F., Timokha, A.N.
'Two-dimensional resonant piston-like sloshing in a moonpool'

Discussor - D.V. Evans:

Why do you need four regions? Surely regions III and IV can be regarded as a single region similar to region I but of finite width?

The problem of two thin barriers has been proved to be unique by Nick Kuznetsov so it would be surprising if the problem of two thick barriers which we have here were non-unique which perhaps explains why you were unable to find any trapped modes.

Reply:

If we want to consider ONLY linear problem, you are right. However, ignoring decomposition in III and IV implies zero-Neumann conditions that are not analytically satisfied on the vertical wall of the hull. Our experience with sloshing says that the asymptotic modal technique is then invalid. One simple reason is that we should calculate higher derivatives of linear solution at the wall and the error will dramatically increase (our linear approximation is found by a variational scheme). However, these higher derivatives determine the hydrodynamic coefficients near nonlinear terms.

Additional arguments, as we found after working with vortex-shedding analysis, this decomposition is necessary for Graham's technique with a local vortex model. If we do not separate III and IV, the maximum error will be expected at the corner (for zero-Neumann condition). This means that our predictions of the vortex shedding will be very-very rough.